

Directional information transfer between interacting Brownian particles

Tenta Tani

Department of Physics, The University of Osaka, Toyonaka, Osaka 560-0043, Japan

(Dated: March 12, 2026)

We theoretically investigate how information flows when two particles interact with each other. Understanding the physical mechanisms of directional information flow is crucial for advancing information thermodynamics and stochastic computing. However, the fundamental connection between mechanical motion and causal information transfer remains elusive. To focus only on essential effects of physical dynamics, we examine two interacting Brownian particles confined in a one-dimensional potential. By simulating their Langevin dynamics, we quantify the causal information exchange using transfer entropy. We demonstrate that a mass asymmetry inherently breaks the symmetry of information flow, inducing a net directional transfer from the heavier to the lighter particle. Physically, the heavier particle, possessing larger inertia and higher active information storage, retains the memory of its trajectory longer against thermal fluctuations, thereby acting as a source of information. We analytically clarify that this net transfer is governed by a competition between the difference in memory capacity and the predictability of the particle trajectories. Furthermore, we reveal that the net information flow scales logarithmically with the mass ratio. These findings provide essential insights into the physical significance of transfer entropy and the nature of information flow in general physical systems.

I. INTRODUCTION

Directional flow of information has gained increasing importance across various scientific disciplines in recent years. In the context of information theory, the quantitative evaluation of directional information transfer was pioneered by Schreiber [1] through the introduction of transfer entropy (TE). In Ref. [1], the information flow between heartbeat and breathing was examined by the notion of TE; by comparing the magnitude of TE from the heart rate to the breathing rate with that in the reverse direction, a directional information flow was revealed. Since then, this framework has been widely applied to analyze the dynamics of diverse complex systems, ranging from neural systems [2–7] to stock markets [8, 9].

In physics, information thermodynamics [10–20] has become increasingly important in recent years. One of the most intriguing consequences of information thermodynamics is the equivalence of information and work, as demonstrated by the resolution of Maxwell’s demon paradox [14–18, 21–24]. An information-theoretical quantity called mutual information is associated with work; the TE is a type of mutual information. The TE, a measure of information flow, is also an important quantity in information thermodynamics [25–41].

From a practical standpoint, information flow is crucial in the emerging field of stochastic computing [23, 42–44]. Despite the growing attention to such applications, the fundamental relationship between the underlying physical motion of particles and the resulting information flow has not yet been elucidated. It is not clear how information is transferred through particle collisions, and more generally, how we can interpret the TE in physical systems. By elucidating these problems in simpler physical systems, we can apply information flow concepts to various physical systems including nanoparticles in liquids and molecules in gases. Ultimately, studies of the TE in

these systems are essential to strengthen the connection between information theory and physics.

Recently, we examined the meaning and role of the TE in magnetic skyrmions confined in a box both theoretically [45] and experimentally [46], motivated by their potential application as information carriers, or “skyrmion bits” [44, 46] towards ultralow-power stochastic computing. However, in these studies, the system parameters were fixed in principle. Most notably, the two interacting particles were treated as identical, which naturally leads to a perfectly symmetric information exchange, i.e., $T_{X \rightarrow Y} = T_{Y \rightarrow X}$. Furthermore, skyrmion dynamics inevitably involve gyrotropic motion originating from their nontrivial topological properties [47–49]. This inherent complexity obscures the underlying fundamental connection between mechanical motion and information transfer. While efficiency of information flow between nonequilibrium Brownian particles driven by a temperature difference has been studied [50], the purely mechanical effects remain unexplored. Specifically, it is still unknown how a difference in inertia (mass) between interacting particles under a uniform thermal environment dictates the causal directionality of information transfer.

In this paper, to reveal the essential relationship between physical motions and information transfer, we focus on one of the simplest setups: two interacting asymmetric Brownian particles confined within a one-dimensional wall potential. By describing the system with coupled Langevin equations and quantifying the causal information flow via TE, we demonstrate that a mass asymmetry inherently induces a directional asymmetry in the information exchange. We reveal that net information (the difference of TEs in both directions, $T_{Y \rightarrow X} - T_{X \rightarrow Y}$) predominantly flows from the particle with larger inertia to the one with smaller inertia. The heavier particle is less susceptible to thermal fluctuations and thus retains the memory of its past trajectory for

a longer duration. It acts as a stable source of information, which is quantitatively supported by its higher active information storage (AIS) [51]. Furthermore, we analytically establish a direct mathematical connection between the directional information flow and the memory capacity. By decomposing the net information flow, we explicitly show that this causal directionality is governed by a competition between the difference in AIS and the difference in the predictability of the particle trajectories (conditional Shannon entropy). Crucially, we clarify that conventional symmetric measures, such as mutual information and correlation functions, merely capture shared mechanical periodicity and fail to detect this causal directionality.

Moreover, we systematically evaluate the mass-ratio dependence of the net information flow, finding that the temporal delay of the information transfer increases with the inertia. Importantly, we establish that the net information flow scales logarithmically with the mass ratio. These results offer a fundamental understanding of the physical meaning of TE and directed information transfer in general physical systems.

The remainder of this paper is organized as follows. In Sec. II, a model of interacting two Brownian particles is introduced. We nondimensionalize the equations of motion to simplify the system description. Section III presents the simulated system dynamics and analyses using information theory. We reveal the nature of net information propagation, which is induced by mass asymmetry. Finally, Sec. IV concludes the paper.

II. MODEL OF BROWNIAN PARTICLES IN ONE-DIMENSIONAL BOX

A. Equations of motion

We consider two interacting Brownian particles, which are labeled by $j = 1, 2$. Their one-dimensional motions are governed by Langevin equations,

$$\begin{aligned} m_1 \frac{d^2 x_1}{dt^2} &= -\gamma \frac{dx_1}{dt} + F_{\text{int}}(x_1, x_2) + F_w(x_1) + R_1, \\ m_2 \frac{d^2 x_2}{dt^2} &= -\gamma \frac{dx_2}{dt} - F_{\text{int}}(x_1, x_2) + F_w(x_2) + R_2, \end{aligned} \quad (1)$$

where x_j is the position of the j th particle. Throughout this paper, we refer to particle 1 and particle 2 as ‘‘particle X’’ and ‘‘particle Y’’, respectively. The parameter γ is a damping coefficient, assumed to be identical for both particles. We model the particle–particle interaction using an exponentially decaying repulsive potential,

$$U_{\text{int}}(x_1, x_2) = U_0 e^{-|x_1 - x_2|/\xi}, \quad (2)$$

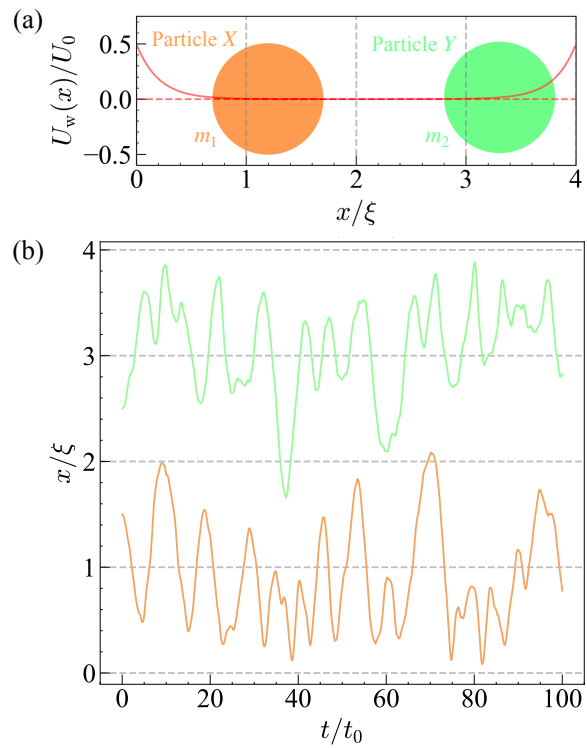


FIG. 1. (a) Snapshot of two interacting Brownian particles (X and Y) in a wall potential. The curve illustrates the potential from the two walls, which vanishes in $1 \leq x/\xi \leq 3$. (b) Trajectories of the two particles, which are well confined between the walls. It is seen that particle X (Y) predominantly exists in the left (right) region because of the repulsive interaction.

where U_0 is the interaction energy and ξ is the interaction range. The force is obtained from this potential,

$$\begin{aligned} F_{\text{int}}(x_1, x_2) &= -\frac{\partial U_{\text{int}}}{\partial x_1} \\ &= \frac{U_0}{\xi} e^{-|x_1 - x_2|/\xi} \text{sgn}(x_1 - x_2). \end{aligned} \quad (3)$$

Here, $\text{sgn}(x)$ denotes the sign function. We assume the walls at $x = 0$ and L that yield an exponentially decaying potentials as well,

$$U_w(r) = U_{w0} [e^{-r/\xi_w} + e^{-(L-r)/\xi_w}], \quad (4)$$

where U_{w0} and ξ_w are the energy scale and interaction range of the wall potential, respectively. The symbol r denotes the particle coordinate. The corresponding wall force is explicitly written as

$$F_w(r) = \frac{U_{w0}}{\xi_w} [e^{-r/\xi_w} - e^{-(L-r)/\xi_w}]. \quad (5)$$

The last term in Eq. (1), R_j , represents the random force originating from thermal fluctuations.

Here, we model both the particle–particle and particle–wall interactions using exponentially decaying functions for both physical and computational reasons. Physically, these exponential forms generically capture soft short-range repulsions, which are realized in interacting quasiparticles such as magnetic skyrmions [45, 52–55], for instance. Computationally, unlike hard-core or algebraically diverging potentials (e.g., the Lennard–Jones potential), exponential potentials do not exhibit singularities at zero distance. This softness is highly advantageous in Langevin dynamics simulations, as it prevents unphysical numerical instabilities that could otherwise occur when random thermal fluctuations occasionally drive the particles extremely close to each other or to the walls.

To simplify the form and concentrate on the fundamental physics, we nondimensionalize the Langevin equations [Eq. (1)]. We choose m_1 , U_0 , and ξ as the basic units of mass, energy, and length, respectively. Consequently, the characteristic unit of time is defined as $t_0 \equiv \xi\sqrt{m_1/U_0}$. Equation (1) is then simplified as

$$\begin{aligned} \frac{d^2\hat{x}_1}{d\hat{t}^2} &= -\hat{\gamma}\frac{d\hat{x}_1}{d\hat{t}} + e^{-|\hat{x}_1-\hat{x}_2|}\text{sgn}(\hat{x}_1-\hat{x}_2) \\ &\quad + \frac{\hat{U}_{w0}}{\hat{\xi}_w}[e^{-\hat{x}_1/\hat{\xi}_w} - e^{-(\hat{L}-\hat{x}_1)/\hat{\xi}_w}] + \hat{R}_1, \\ \mu\frac{d^2\hat{x}_2}{d\hat{t}^2} &= -\hat{\gamma}\frac{d\hat{x}_2}{d\hat{t}} - e^{-|\hat{x}_1-\hat{x}_2|}\text{sgn}(\hat{x}_1-\hat{x}_2) \\ &\quad + \frac{\hat{U}_{w0}}{\hat{\xi}_w}[e^{-\hat{x}_2/\hat{\xi}_w} - e^{-(\hat{L}-\hat{x}_2)/\hat{\xi}_w}] + \hat{R}_2, \end{aligned} \quad (6)$$

where $\hat{x}_j \equiv x_j/\xi$ and $\hat{t} \equiv t/t_0$ are the dimensionless position and time, respectively. We define dimensionless parameters $\hat{\gamma} \equiv \gamma(\xi/\sqrt{m_1U_0})$, $\hat{U}_{w0} \equiv U_{w0}/U_0$, $\hat{\xi}_w \equiv \xi_w/\xi$, and $\hat{L} = L/\xi$. To introduce mass asymmetry, we set $m_1 \neq m_2$, which yields a mass ratio $\mu \equiv m_2/m_1 \neq 1$. The dimensionless random force \hat{R}_j satisfies the fluctuation–dissipation theorem and is discretized in our numerical simulations as

$$\hat{R}_j = \sqrt{\frac{2\hat{\gamma}\hat{T}}{\delta\hat{t}}}\mathcal{N}(0,1), \quad (7)$$

where $\mathcal{N}(0,1)$ is a random variable drawn from the standard normal distribution. Here, $\hat{T} \equiv k_B T/U_0$ is the dimensionless temperature, and $\delta\hat{t}$ represents the discrete dimensionless time step.

B. Particle dynamics

Figure 1(a) shows a schematic picture of two Brownian particles (particle X and Y) confined in a box. The vertical axis is the wall potential U_w with $\hat{L} = 4$. In order to investigate the effect of interaction, we use parameter values $\hat{U}_{w0} = 0.5$ and $\hat{\xi}_w = 0.2$, which renders the wall

potential negligibly small ($U_w \approx 0$) in the central range of $1 \leq x/\xi \leq 3$.

In the numerical simulation of Eq. (6), we use the fourth-order Runge–Kutta method, which corresponds to the Stratonovich calculus. Since the coefficient of the random force $\sqrt{2\hat{\gamma}\hat{T}/\delta\hat{t}}$ is constant (the system is driven by additive noise), the Itô and Stratonovich calculus yield the same results. The simulation time is $t_f = 100t_0$ with time increment of $\delta\hat{t} = 0.1$. We employ the temperature parameter $\hat{T} = 0.1$, and the damping constant is fixed to be $\hat{\gamma} = 0.3$. In Fig. 1(b), we illustrate the dynamics of the system with $\mu = 1$ (two identical particles). At $t = 0$, the particles are released from rest at $\hat{x}_1 = 1.5$ and $\hat{x}_2 = 2.5$. As shown in Fig. 1(b), the two particles are well confined within the box ($0 \leq x/\xi \leq 4$) and clearly exhibit mutual repulsion.

Throughout the paper, we fix the above parameters ($\hat{\gamma}$, \hat{U}_{w0} , $\hat{\xi}_w$, \hat{L} , \hat{T}) while varying the mass ratio μ , which serves as the sole source of symmetry breaking between the particles. Note that in realistic experimental settings involving colloidal or nanoparticles, the mass and the friction coefficient are generally coupled. However, if both parameters were varied simultaneously, it would be difficult to disentangle whether the asymmetric information flow originates from the difference in inertia or the difference in damping coefficient. Therefore, to unambiguously isolate the purely mechanical effect of inertia, we theoretically treat the friction and the mass as independent parameters and assign an identical $\hat{\gamma}$ to both particles. This idealization allows us to establish that mass asymmetry alone is fundamentally sufficient to induce a directed causal information transfer.

III. INFORMATION-THEORETICAL ANALYSIS

A. Shannon entropy

To analyze the flow of information between the particles, we numerically simulate the Langevin equations [Eq. (6)] $N = 10^6$ times. This ensemble size sufficiently suppresses statistical errors and enables the following analyses of information flow. From each calculation, we obtain two time series,

$$\begin{aligned} \{\hat{x}_1^{(i)}(0), \hat{x}_1^{(i)}(t_0\delta\hat{t}), \hat{x}_1^{(i)}(2t_0\delta\hat{t}), \dots, \hat{x}_1^{(i)}(t_f)\}, \\ \{\hat{x}_2^{(i)}(0), \hat{x}_2^{(i)}(t_0\delta\hat{t}), \hat{x}_2^{(i)}(2t_0\delta\hat{t}), \dots, \hat{x}_2^{(i)}(t_f)\}, \end{aligned} \quad (8)$$

where $i = 1, 2, \dots, N$ specifies an individual simulation.

For the calculation of entropic quantities, we discretize the position as

$$\begin{aligned} \text{Cell 0: } &x/\xi < 1 \\ \text{Cell 1: } &1 \leq x/\xi < 2 \\ \text{Cell 2: } &2 \leq x/\xi < 3 \\ \text{Cell 3: } &x/\xi > 3 \end{aligned} \quad (9)$$

as shown in Fig. 1(a). Because of the wall potential, the particles rarely move inside the walls: $x/\xi < 0$ and $x/\xi > 4$. Under this criterion, after executing N simulations, we discretize the positions as

$$\begin{aligned} \hat{x}_1^{(i)}(t) &\rightarrow a_t^{(i)} \in \{0, 1, 2, 3\}, \\ \hat{x}_2^{(i)}(t) &\rightarrow b_t^{(i)} \in \{0, 1, 2, 3\}, \end{aligned} \quad (10)$$

where a_t and b_t are the discrete spatial states of particle X and Y , respectively. We define the corresponding stochastic variables as X_t and Y_t , which take the values a_t and b_t .

The probability that particle X exists in cell a_t at time t is given by

$$p(a_t) = \frac{1}{N} \sum_{i=1}^N \delta(a_t^{(i)} - a_t), \quad (11)$$

where $\delta(x)$ is Kronecker's delta,

$$\delta(x) = \begin{cases} 1 & (x = 0) \\ 0 & (x \neq 0). \end{cases} \quad (12)$$

Similarly, the joint probability between different times t and t' is written as

$$p(a_t, a_{t'}) = \frac{1}{N} \sum_{i=1}^N \delta(a_t^{(i)} - a_t) \delta(a_{t'}^{(i)} - a_{t'}), \quad (13)$$

and the conditional probability is obtained from the relation $p(a_t | a_{t'}) = p(a_t, a_{t'})/p(a_{t'})$.

For particles X and Y , the Shannon entropy at time t is written as

$$\begin{aligned} H(X_t) &= - \sum_{a_t=0}^3 p(a_t) \ln p(a_t), \\ H(Y_t) &= - \sum_{b_t=0}^3 p(b_t) \ln p(b_t), \end{aligned} \quad (14)$$

which represents the randomness of a particle's position. Figure 2 illustrates the time evolution of Shannon entropies $H(X_t), H(Y_t)$ for $\mu = 1$ and 2. In Fig. 2(a), we show the symmetric case, $\mu = 1$. As expected, the two entropy curves are almost perfectly identical. The initial rapid increase in H corresponds to the expansion of the probability distribution from a deterministic initial state that is driven by the repulsive interaction and thermal fluctuations. The subsequent oscillations reflect the following processes: the expanding distribution hits the soft wall potentials and bounces back, causing a transient spatial localization of the particles. The vertical dashed line indicates the characteristic time scale $\tau_{\text{th}} \equiv \xi/v_{\text{th}}$ [45], where v_{th} is the thermal velocity defined as

$$v_{\text{th}} = \sqrt{\frac{k_{\text{B}}T}{m_1}}. \quad (15)$$

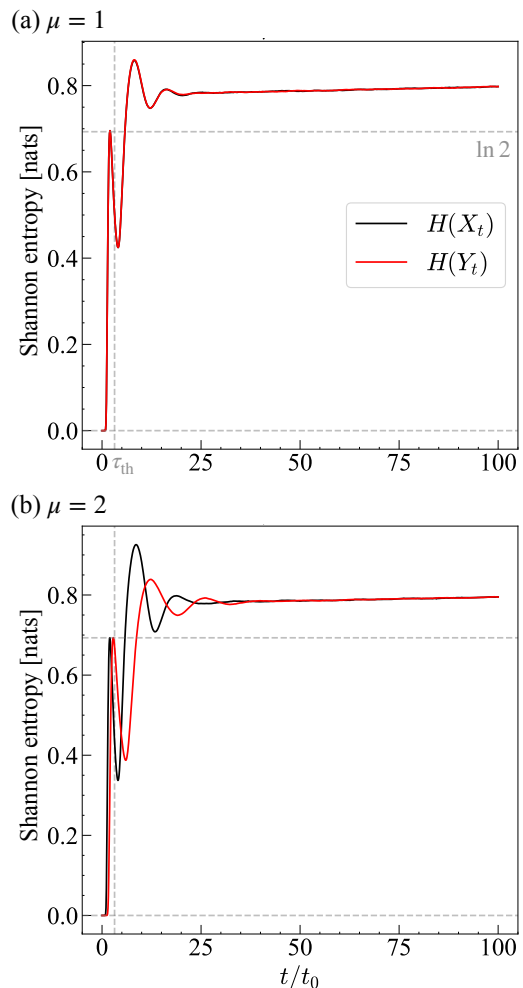


FIG. 2. (a) Time evolution of Shannon entropy $H(X_t)$ (particle X) and $H(Y_t)$ (particle Y) for mass parameter $\mu = 1$ (identical particles). The vertical line, $\tau_{\text{th}} = \xi/v_{\text{th}}$, represents the characteristic time of thermal motion (see the text). (b) Similar plots for an asymmetric case $\mu = 2$ (Y is twice heavier than X).

It can be seen that this rebound process occurs on the order of τ_{th} . After the initial transient oscillations are damped out ($t/t_0 \gtrsim 25$), the Shannon entropies reach a steady state, which gives $H \approx 0.8$. This value is slightly larger than $\ln 2$ (horizontal dashed line); although a particle is predominantly localized in two out of the four cells (i.e., cell 0 and 1 for particle X), it sometimes has a chance to explore the adjacent cell (cell 2). The effective volume occupied by a single particle can be estimated as $\hat{L}_{\text{eff}} = e^{0.8} \approx 2.2$ cells.

Figure 2(b) shows a similar plot for the asymmetric case, $\mu = 2$. We clearly see that the oscillation of particle Y (heavier particle) becomes slower with a smaller amplitude compared to particle X . This represents its larger inertia. The probability distribution of the heavier particle expands and localizes more gradually than that of the

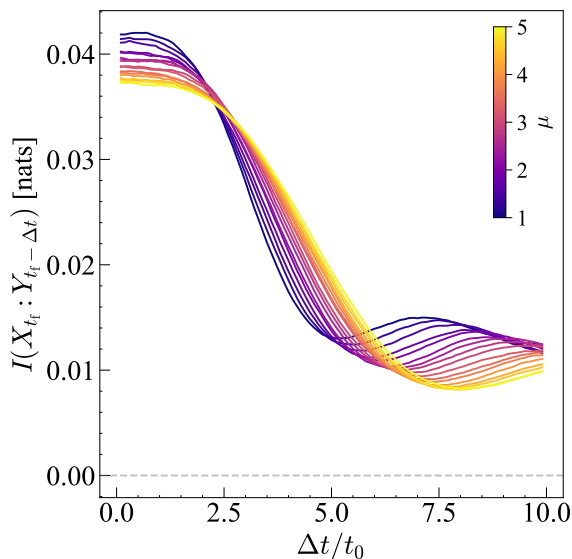


FIG. 3. Mutual information $I(X_t : Y_{t-\Delta t})$ at the reference time $t = t_f$, illustrated as a function of the time lag Δt . The mass ratio μ varies from $\mu = 1$ to 5.

lighter one. The relaxation process takes longer than in the symmetric case; both particles reach a steady state for $t/t_0 \gtrsim 40$.

B. Mutual information and active information storage

Here, by calculating mutual information $I(X_t : Y_{t-\Delta t})$, we examine how the states of the two particles depend on each other. The mutual information is defined as

$$\begin{aligned} I(X_t : Y_{t-\Delta t}) &= H(X_t) - H(X_t | Y_{t-\Delta t}) \\ &= \sum_{a_t, b_{t-\Delta t}=0}^3 p(a_t, b_{t-\Delta t}) \ln \frac{p(a_t, b_{t-\Delta t})}{p(a_t)p(b_{t-\Delta t})}, \end{aligned} \quad (16)$$

where conditional Shannon entropy $H(X_t | Y_{t-\Delta t})$ is given by

$$H(X_t | Y_{t-\Delta t}) = - \sum_{a_t, b_{t-\Delta t}=0}^3 p(a_t, b_{t-\Delta t}) \ln p(a_t | b_{t-\Delta t}). \quad (17)$$

Mutual information $I(X_t : Y_{t-\Delta t})$ represents information shared between particle X at time t (X_t) and particle Y at time $t - \Delta t$ ($Y_{t-\Delta t}$). For large time delay Δt , X_t and $Y_{t-\Delta t}$ become uncorrelated, giving $H(X_t | Y_{t-\Delta t}) = H(X_t)$ and therefore $I(X_t : Y_{t-\Delta t}) = 0$ (no shared information).

Figure 3 illustrates the Δt dependence of the mutual information for several values of mass ratio μ . In order to examine steady states, we fix the reference time to $t = t_f$. The stochastic motion of either particle degrades

the shared information over time. Thus, the mutual information, rapidly decays as the time lag Δt increases. Crucially, the decay rate strongly depends on the mass ratio. For the symmetric case ($\mu = 1$), the mutual information exhibits a relatively fast decay accompanied by a transient oscillation around $\Delta t/t_0 \approx 7.5$, reflecting the rapid rebound process against the walls (see Sec. III A). In contrast, as the mass ratio μ increases, the heavier particle Y possesses a larger inertia, which significantly slows down its dynamics. Consequently, the memory of its past state is preserved for a longer duration, leading to a much slower decay of the mutual information.

As pointed out in Ref. [20], $(I(X_t : Y_{t-\Delta t}) - I(X_t : Y_t))/\Delta t$ expresses an internal information flow, which realize an observation and a feedback process in the system (Maxwell's demon's task). In our system, the initial slopes in Fig. 3 is zero, showing the absence of the Maxwell's demon.

While these observations provide physical insights into the correlation times of the system, the mutual information $I(X_t : Y_{t-\Delta t})$ itself is fundamentally a symmetric measure; it only quantifies the shared information between two variables and cannot distinguish whether the correlation arises from X influencing Y , or Y influencing X . Therefore, the mutual information lacks the ability to detect the directionality of information flow [1]. Similarly, a conventional correlation function only captures the shared mechanical periodicity and fails to reveal the causal directionality (see Appendix A for detailed discussions). To reveal the true causal influence and the directional flow of information driven by the mass asymmetry, we must turn to a more sophisticated measure, TE.

Before analyzing the information transfer between the two particles using the TE, it is instructive to first quantify how much information each particle internally retains about its own past. For this purpose, we evaluate the AIS [51],

$$\begin{aligned} A_X(\Delta t) &= I(X_t : X_{t-\Delta t}), \\ A_Y(\Delta t) &= I(Y_t : Y_{t-\Delta t}), \end{aligned} \quad (18)$$

which measures the predictable information from a particle's past state to its present state. Figure 4 shows the AIS for both particles as a function of the lag Δt at the reference time $t = t_f$. As the time lag Δt increases, from the initial values $A_X(\Delta t = 0) = H(X_t)$ and $A_Y(\Delta t = 0) = H(Y_t)$, the AIS drops to zero. As the mass ratio μ increases, the AIS of the lighter particle X [Fig. 4(a)] remains almost unchanged, whereas the decay rate for the heavier particle Y [Fig. 4(b)] decreases. In other words, the heavier particle Y consistently exhibits a higher AIS than the lighter particle X . This quantitatively confirms our previous observation from the mutual information: the larger inertia of Y can retain a stronger memory of its own trajectory.

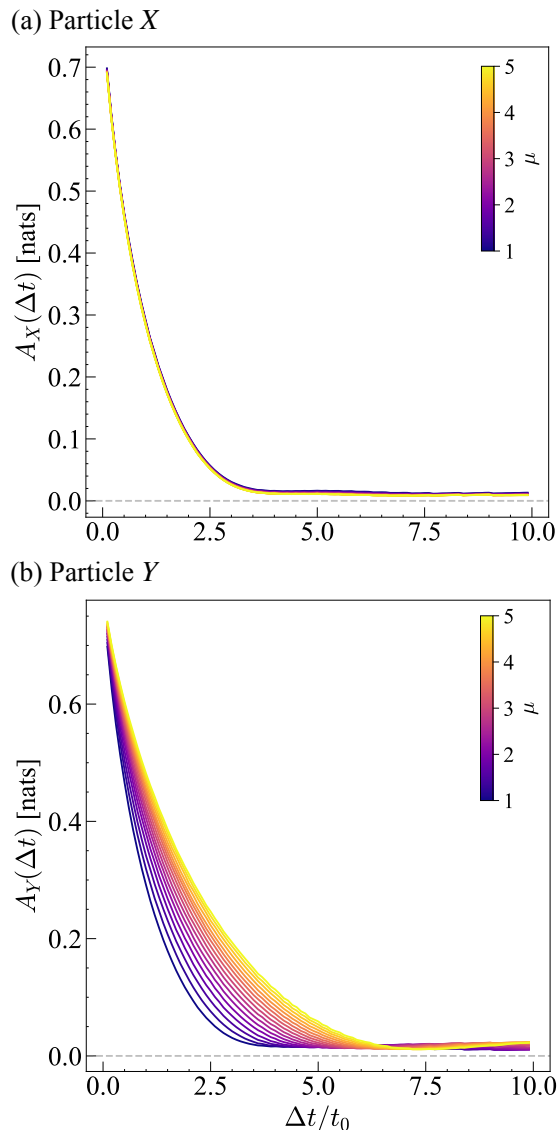


FIG. 4. Active information storage of particle X [panel (a), lighter] and Y [panel (b), heavier], as a function of the time lag Δt . The mass ratio μ is varied from 1 to 5.

C. Transfer entropy

Having established that the heavier particle (particle Y) acts as a more stable source of information (higher AIS) while the lighter particle (particle X) is more susceptible to thermal fluctuations, the crucial question arises: does this asymmetry in memory lead to a directional flow of information between them? To answer this, we calculate the TE, which quantifies the amount of directed information transferred from a source variable to a target variable. The TE from particle Y to particle X with a

time lag Δt is defined as

$$\begin{aligned} T_{Y \rightarrow X}(\Delta t) &= I(X_t : Y_{t-\Delta t} | X_{t-\Delta t}) \\ &= H(X_t | X_{t-\Delta t}) - H(X_t | X_{t-\Delta t}, Y_{t-\Delta t}), \end{aligned} \quad (19)$$

which measures how much the past state of Y (at time $t - \Delta t$) reduces the uncertainty about the present state of X (at time t), given the past state of X itself. The TE is a widely used measure of information flow [2–9, 25–33, 56–58]. From the TE in both directions, $T_{Y \rightarrow X}(\Delta t)$ and $T_{X \rightarrow Y}(\Delta t)$, we can calculate the net TE [6, 7, 9, 56, 58],

$$T_{\text{net}}(\Delta t) = T_{Y \rightarrow X}(\Delta t) - T_{X \rightarrow Y}(\Delta t), \quad (20)$$

to determine the dominant direction of the information flow. While Eq. (20) provides the operational definition of the net information flow, its fundamental significance is governed by an information-theoretic sum rule, Eq. (22). In a stationary state, the total uncertainty (Shannon entropy) of each particle is decomposed into its internal memory (AIS), the incoming information flow (TE), and the conditional Shannon entropy [Eq. (22)]. As we will derive in Eq. (23), the mirror symmetry of our system enforces a balance between these components, revealing that T_{net} is intrinsically driven by the asymmetry in the particles' memory capacities.

Figure 5 displays the time-lag dependence of the TEs, $T_{Y \rightarrow X}$ and $T_{X \rightarrow Y}$, along with their difference (net TE) T_{net} , for three selected mass ratios: (a) $\mu = 1$, (b) $\mu = 2$, and (c) $\mu = 3$. Similar to the analysis in Sec. III B, we fix the reference time to $t = t_f$ to examine the steady-state information transfer. For the identical particles [Fig. 5(a)], the two curves $T_{Y \rightarrow X}$ and $T_{X \rightarrow Y}$ almost overlap. As a result, T_{net} fluctuates strictly within the statistical noise level $\pm 1/\sqrt{N}$ (shaded region), confirming the absence of a preferred direction. The peak time of the TEs ($T_{Y \rightarrow X}$ and $T_{X \rightarrow Y}$) is slightly shorter than τ_{th} . This shift could be attributed to the repulsive interaction U_{int} , which accelerates the particles and consequently shortens the effective interaction time scale. The situation is different from a two-skyrmion system confined within a square box [45], in which the TE peak positions coincide with τ_{th} . In the two-skyrmion case, because of the gyrotropic force, the repulsive interaction results primarily in tangential circular motion rather than radial motion.

As the mass asymmetry is introduced and increased [Fig. 5(b) and (c)], the flow from the heavier particle Y to the lighter particle X ($T_{Y \rightarrow X}$) becomes larger than the reverse flow ($T_{X \rightarrow Y}$). Consequently, T_{net} clearly emerges from the noise floor, forming a distinct positive peak. This explicitly visualizes the growth of the directed information transfer driven by the mass difference. We can conclude that, from the heavier particle Y which retains more information [higher AIS, Fig. 4(b)], net information flows to the lighter particle X.

In each panel of Fig. 5, the peak positions of all the three curves are almost the same. As μ increases, the peaks are shifted to larger Δt . This behavior can be interpreted as a result of the increased inertia of particle Y,

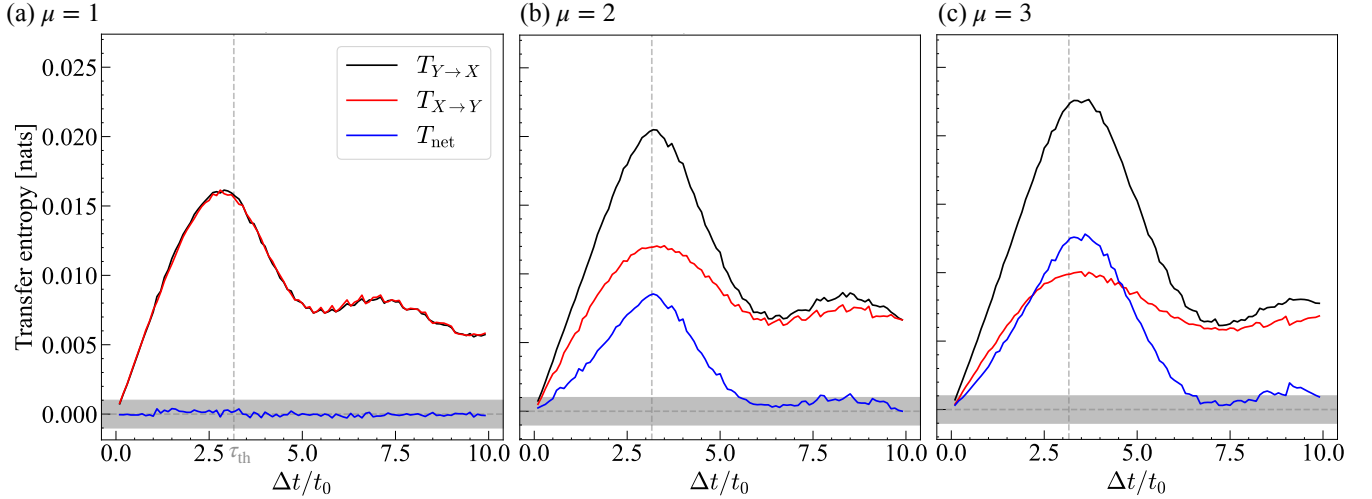


FIG. 5. Transfer entropies $T_{Y \rightarrow X}$, $T_{X \rightarrow Y}$, and their difference T_{net} for (a) $\mu = 1$, (b) $\mu = 2$, and (c) $\mu = 3$. The shaded region illustrates the statistical noise level $\pm 1/\sqrt{N}$. The vertical dashed lines represent the characteristic time scale of thermal motions, τ_{th} (see the text).

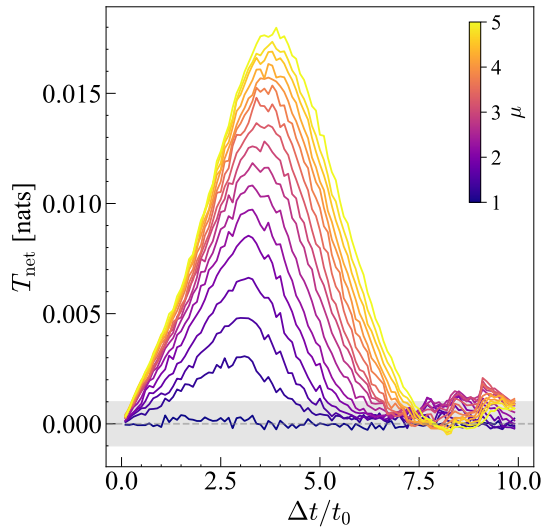


FIG. 6. Net transfer entropy T_{net} for various mass ratios μ , as a function of the time lag Δt . The shaded region represents the statistical noise $\pm 1/\sqrt{N}$.

which slows down the system's dynamics and thereby delays the propagation of physical influence from the heavier particle to the lighter one.

To systematically capture this growth across a continuous range of mass asymmetry, Fig. 6 shows the net TE, T_{net} , for various mass ratios μ . As μ increases, the peak position continuously shifts to larger Δt . Simultaneously, the peak height systematically increases, indicating that a heavier particle acts as a more robust source of information. Comparing the mutual information (Fig. 3) and

the transfer entropy (Fig. 6) for various mass ratios μ , we see that the decay of mutual information is faster than that of the TE peak. This is because the random motion of either particle decreases the mutual information, as mentioned in Sec. III B.

To explicitly understand what drives this robust peak in the net TE, we examine the mathematical connection between the memory difference (AIS) and the resulting directional information flow (net TE). From the definition of AIS [Eq. (18)], we have

$$\begin{aligned} A_X(\Delta t) &= H(X_t) - H(X_t | X_{t-\Delta t}), \\ A_Y(\Delta t) &= H(Y_t) - H(Y_t | Y_{t-\Delta t}). \end{aligned} \quad (21)$$

By using the definition of TE [Eq. (19)], we can rewrite the Shannon entropies as

$$\begin{aligned} H(X_t) &= A_X(\Delta t) + T_{Y \rightarrow X}(\Delta t) + H(X_t | X_{t-\Delta t}, Y_{t-\Delta t}), \\ H(Y_t) &= A_Y(\Delta t) + T_{X \rightarrow Y}(\Delta t) + H(Y_t | X_{t-\Delta t}, Y_{t-\Delta t}). \end{aligned} \quad (22)$$

Assuming that the steady state is realized for sufficiently large t (see Fig. 2), we write $H(X_t) = H(Y_t)$. Therefore, we obtain

$$T_{\text{net}}(\Delta t) = \delta A + \delta H_c, \quad (23)$$

where we define

$$\begin{aligned} \delta A &\equiv A_Y(\Delta t) - A_X(\Delta t), \\ \delta H_c &\equiv H(Y_t | X_{t-\Delta t}, Y_{t-\Delta t}) - H(X_t | X_{t-\Delta t}, Y_{t-\Delta t}). \end{aligned} \quad (24)$$

Equation (23) clearly states that the net TE consists of two components: the difference in AIS and in conditional Shannon entropy. The first component $\delta A = A_Y(\Delta t) - A_X(\Delta t)$ is illustrated in Fig. 7, for several mass ratios μ . The shapes of these curves closely resemble the

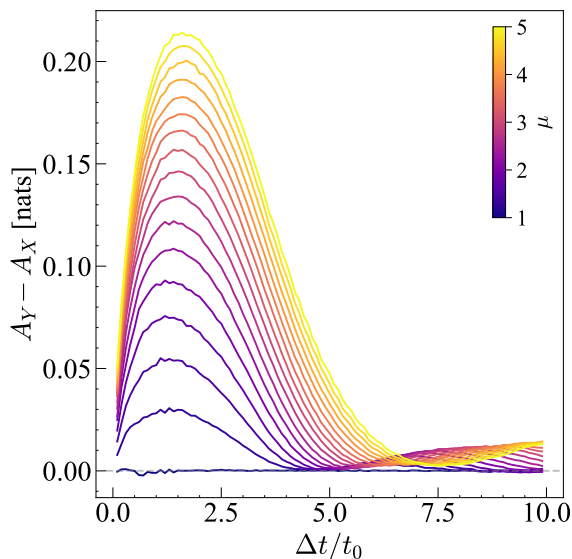


FIG. 7. Difference of active information storage $\delta A = A_Y - A_X$ as a function of the time lag Δt . The mass ratio μ varies from 1 to 5.

structures of the net TE, $T_{\text{net}}(\Delta t)$ (Fig. 6), directly supporting our claim that the difference in memory capacity (AIS) inherently drives the directional information propagation.

However, a comparison between Fig. 6 and Fig. 7 reveals a significant difference in magnitude: the AIS difference is approximately an order of magnitude larger than the net TE. This difference is precisely compensated by the second component in Eq. (23), δH_c . Given the past states of both particles ($X_{t-\Delta t}, Y_{t-\Delta t}$), the heavier particle Y , due to its larger inertia, tends to exhibit a more predictable trajectory compared to the lighter particle X . Consequently, the conditional uncertainty of Y is strictly smaller than that of X , resulting in $\delta H_c < 0$. Thus, this negative δH_c term strongly decreases the raw memory difference δA , leaving the smaller yet distinct positive net information flow T_{net} from the heavier to the lighter particle.

To further characterize the impact of mass asymmetry on the directional transfer of information, we extract the maximum value of the net TE,

$$T_{\text{net}}^{(\max)} = \max_{\Delta t} [T_{\text{net}}(\Delta t)], \quad (25)$$

and plot it against the mass ratio μ in Fig. 8. The plot clearly reveals that the information flow grows with a decreasing rate as the mass asymmetry increases. To minimally capture this scaling behavior, we apply a single-parameter logarithmic fit, $f(\mu) = A \ln \mu$. As shown in Fig. 8, this simple model well describes the overall trend within the currently investigated range ($1 \leq \mu \leq 5$) with the fitting parameter $A = 0.0115$. Note that the slight scatter of the data points around the fitting curve (e.g.,

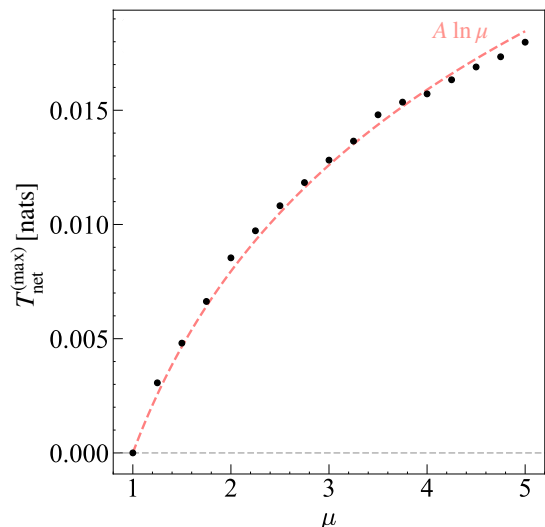


FIG. 8. Maximum value of the net transfer entropy, $T_{\text{net}}^{(\max)}$, plotted against the mass ratio μ . The dashed curve is a logarithmic fit $f(\mu) = A \ln \mu$.

at $\mu = 3.5$) originates from the inherent statistical fluctuations in the TE. As observed in Fig. 6, the net TE, $T_{\text{net}}(\Delta t)$, exhibits minor jaggedness near its peak due to the estimation of joint probabilities from the finite ensemble size ($N = 10^6$). Consequently, extracting the absolute maximum value occasionally captures these local noise spikes rather than the ideal peak value, leading to the observed minor deviations. Nevertheless, these statistical variations are sufficiently small and do not obscure the overall logarithmic dependence of $T_{\text{net}}^{(\max)}$.

This logarithmic scaling can be understood as a phenomenological description of the saturation process towards a deterministic limit. As $\mu \rightarrow \infty$, the heavier particle becomes increasingly deterministic, causing its capacity to transfer causal information to eventually hit an upper bound. Thus, the logarithmic function naturally captures this gradual saturation of information flow driven by the extreme mass asymmetry.

In the preceding analyses, we employed a spatial discretization of $N_{\text{cell}} = 4$ cells for two primary reasons. First, as N_{cell} increases, the computational and data requirements for entropic quantities dramatically escalate. Specifically, evaluating the TE [Eq. (19)] requires estimating the joint probability distribution over $(N_{\text{cell}})^3$ states. Consequently, the ensemble size N required to secure statistical accuracy and suppress finite-sampling biases grows cubically. While simulating a larger N_{cell} is theoretically possible, obtaining such massive datasets is often unrealistic in actual experiments. We deliberately chose $N_{\text{cell}} = 4$ to align with practically feasible experimental setups [46]. Second, if we were to increase N_{cell} , the primary effect would be a quantitative shift of the TE peak to a smaller Δt . For example, $N_{\text{cell}} = 8$ would

yield a peak position slightly shorter than $\tau_{\text{th}}/2$, simply because the spatial distance between adjacent cells is halved ($\xi/2$), thus requiring less time for a particle to traverse. Therefore, although the peak position shifts quantitatively with the spatial resolution, our qualitative conclusion regarding the underlying mechanism of directional information flow remains robust and unaffected by the choice of N_{cell} .

IV. CONCLUSION

In conclusion, we have theoretically investigated the directional information flow between two interacting Brownian particles confined in a one-dimensional potential. By simulating the coupled Langevin equations and evaluating TE, we demonstrated that a mass asymmetry inherently breaks the symmetry of information exchange. Specifically, we revealed that a net information flow emerges, directed consistently from the heavier particle to the lighter one. We found that the TE value increases when the mass ratio increases. This behavior can be understood as follows: the directional information transfer is physically rooted in the difference in inertia. The heavier particle, being less susceptible to thermal fluctuations, retains the memory of its past trajectory for a longer duration, as evidenced by its higher AIS. Consequently, it acts as a stable source of information that continuously influences the stochastic motion of the lighter particle. We analytically pointed out a mathematical connection between the directional information flow (net TE) and the memory (AIS). Specifically, our decomposition of the net TE reveals that this directional flow is governed by a competition between the difference in raw memory capacity (δA) and the difference in predictability of the particle trajectories (δH_c).

The TE peak position is slightly shifted from the thermal characteristic time τ_{th} , unlike the case of a two-skyrmion system confined within a square box [45]. In the two-skyrmion system, a skyrmion-skyrmion interaction results in tangential circular motion; in the case of the one-dimensional Brownian particles, a particle-particle interaction accelerates the particles and gives a TE peak position shorter than τ_{th} .

Furthermore, as demonstrated in our analysis of mutual information, conventional symmetric measures only capture the shared mechanical periodicity of the system and fail to detect this causal directionality. Thus, evaluating TE is essential for isolating the fundamental mechanical effects on information propagation.

Finally, we established that the maximum net TE scales logarithmically with the mass ratio, $T_{\text{net}}^{(\text{max})} \propto \ln \mu$, across the investigated parameter range. We can conclude that the logarithmic behavior naturally captures a leading-order dependence of the net TE $T_{\text{net}}^{(\text{max})}$ on the mass ratio μ ; the net TE should be saturated to a certain finite value for $\mu \rightarrow \infty$.

Our results reveal a clear physical interpretation of TE.

More importantly, these findings provide a fundamental understanding of information flow in general physical systems, including nanoparticles and molecules that exhibit Brownian motion. These insights into directional information flow pave the way to analyze more complex systems such as interacting skyrmion bits driven by topological gyrotropic motion, which hold significant promise for future applications in stochastic computing and nanoscale information processing.

Beyond the specific model of interacting Brownian particles, our findings offer a fundamental perspective on the interpretation of TE in general non-Markovian systems. In the analysis of complex dynamics, a directional information flow is frequently attributed to structural asymmetries, such as unidirectional couplings [1, 59] or feedback mechanisms [20, 33]. However, our results demonstrate that causal directionality can inherently emerge even in systems with perfectly symmetric interactions, driven purely by the asymmetry in memory capacities (AIS). This physically originates from the difference in inertia; purely mechanical differences can manifest as robust causality. This implies that when inferring causal relationships from time-series data, it is crucial to account for the disparate physical timescales or ‘‘inertia’’ of individual components. Our study thus provides a vital physical baseline for TE analyses of general non-Markovian complex systems.

ACKNOWLEDGMENTS

This work was supported by Japan JSPS KAKENHI Grant No. JP23KJ1497. We thank Eiiti Tamura, Yoshishige Suzuki, and Soma Miki for fruitful discussions.

Appendix A: Correlation function

In this appendix, we numerically show that the correlation function cannot capture causal information flow. We define the fluctuations of the discrete spatial states from their ensemble averages as

$$\begin{aligned}\delta a_t^{(i)} &= a_t^{(i)} - \langle a_t \rangle, \\ \delta b_t^{(i)} &= b_t^{(i)} - \langle b_t \rangle.\end{aligned}\tag{A1}$$

The correlation function is then given by

$$C(\Delta t) = \frac{1}{N} \sum_{i=1}^N \delta a_t^{(i)} \delta b_{t-\Delta t}^{(i)},\tag{A2}$$

which vanishes for sufficiently large time delay Δt .

Figure 9 illustrates the correlation functions $C(\Delta t)$ for both symmetric ($\mu = 1$) and asymmetric ($\mu = 2, 3$) cases with $t = t_f$. The curves exhibit damped oscillations characterized by alternating positive peaks and negative valleys. These oscillatory structures merely reflect the periodic bouncing of the particles within the confinement

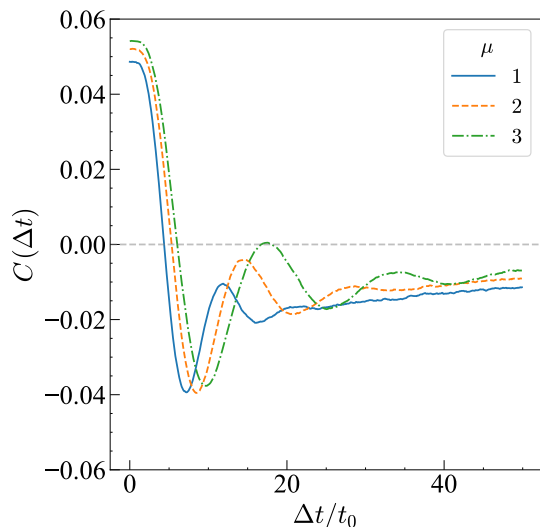


FIG. 9. Correlation functions $C(\Delta t)$ for mass ratios $\mu = 1, 2,$ and 3 .

potentials [see Fig. 2 in the main text]. As μ increases, the oscillation period lengthens simply due to the larger inertia of the heavier particle. Crucially, these peaks appear even in the perfectly symmetric case ($\mu = 1$) where no net directional information flow can physically exist. Furthermore, increasing the mass asymmetry ($\mu > 1$) does not generate any distinct feature representing causal directionality. These results clearly demonstrate that the conventional correlation function only captures the shared mechanical periodicity and is fundamentally incapable of isolating the true causal asymmetry and directional information transfer driven by the mass difference.

-
- [1] T. Schreiber, Measuring information transfer, *Phys. Rev. Lett.* **85**, 461 (2000).
- [2] R. Kobayashi and K. Kitano, Impact of network topology on inference of synaptic connectivity from multi-neuronal spike data simulated by a large-scale cortical network model, *J. Comput. Neurosci.* **35**, 109 (2013).
- [3] M. Kawasaki, Y. Uno, J. Mori, K. Kobata, and K. Kitajo, Transcranial magnetic stimulation-induced global propagation of transient phase resetting associated with directional information flow, *Front. hum. neurosci.* **8** (2014).
- [4] M. Staniek and K. Lehnertz, Symbolic transfer entropy, *Phys. Rev. Lett.* **100**, 158101 (2008).
- [5] R. Vicente, M. Wibral, M. Lindner, and G. Pipa, Transfer entropy—a model-free measure of effective connectivity for the neurosciences, *J. Comput. Neurosci.* **30**, 45 (2011).
- [6] S. Sabesan, L. B. Good, K. S. Tsakalis, A. Spanias, D. M. Treiman, and L. D. Iasemidis, Information flow and application to epileptogenic focus localization from intracranial eeg, *IEEE Trans. Neural Syst. Rehabil. Eng.* **17**, 244 (2009).
- [7] V. A. Vakorin, B. Misic, O. Krakovska, and A. R. McIntosh, Empirical and theoretical aspects of generation and transfer of information in a neuromagnetic source network, *Front. syst. neurosci.* **5** (2011).
- [8] O. Kwon and J.-S. Yang, Information flow between stock indices, *Europhys. Lett.* **82**, 68003 (2008).
- [9] R. Marschinski and H. Kantz, Analysing the information flow between financial time series: An improved estimator for transfer entropy, *Eur. Phys. J. B* **30**, 275 (2002).
- [10] J. M. Parrondo, J. M. Horowitz, and T. Sagawa, Thermodynamics of information, *Nat. Phys.* **11**, 131 (2015).
- [11] D. Andrieux and P. Gaspard, Nonequilibrium generation of information in copolymerization processes, *Proc. Natl. Acad. Sci. USA* **105**, 9516 (2008).
- [12] C. Jarzynski, The thermodynamics of writing a random polymer, *Proc. Natl. Acad. Sci. USA* **105**, 9451 (2008).
- [13] K. Hayashi, H. Ueno, R. Iino, and H. Noji, Fluctuation theorem applied to f_1 -atpase, *Phys. Rev. Lett.* **104**, 218103 (2010).
- [14] T. Sagawa and M. Ueda, Second law of thermodynamics with discrete quantum feedback control, *Phys. Rev. Lett.* **100**, 080403 (2008).
- [15] T. Sagawa and M. Ueda, Minimal energy cost for thermodynamic information processing: Measurement and information erasure, *Phys. Rev. Lett.* **102**, 250602 (2009).
- [16] T. Sagawa and M. Ueda, Generalized Jarzynski equality under nonequilibrium feedback control, *Phys. Rev. Lett.* **104**, 090602 (2010).
- [17] T. Sagawa and M. Ueda, Fluctuation theorem with information exchange: Role of correlations in stochastic thermodynamics, *Phys. Rev. Lett.* **109**, 180602 (2012).
- [18] T. Sagawa and M. Ueda, Role of mutual information in entropy production under information exchanges, *New J. Phys.* **15**, 125012 (2013).
- [19] J. Karbowski, Information thermodynamics: From physics to neuroscience, *Entropy* **26** (2024).
- [20] J. M. Horowitz and M. Esposito, Thermodynamics with continuous information flow, *Phys. Rev. X* **4**, 031015 (2014).
- [21] L. Szilard, Über die Entropieverminderung in einem thermodynamischen System bei Eingriffen intelligenter Wesen, *Z. Phys.* **53**, 840 (1929).
- [22] L. Brillouin, Maxwell’s demon cannot operate: Information and entropy. I, *J. Appl. Phys.* **22**, 334 (1951).
- [23] C. H. Bennett, The thermodynamics of computation—a review, *Int. J. Theor. Phys.* **21**, 905 (1982).
- [24] R. Landauer, Irreversibility and heat generation in the computing process, *IBM J. Res. Dev.* **5**, 183 (1961).
- [25] A. Roza, J. Morales, J. Moeyersons, R. Joshi, E. G. Ciani, P. Borzée, B. Buyse, D. Testelmans, S. Van Huffel, and C. Varon, Benchmarking transfer entropy methods

- for the study of linear and nonlinear cardio-respiratory interactions, *Entropy* **23** (2021).
- [26] L. Sandoval Jr, Structure of a global network of financial companies based on transfer entropy, *Entropy* **16**, 4443 (2014).
- [27] M. J. Falkowski and P. D. Domański, Causality analysis with different probabilistic distributions using transfer entropy, *Appl. Sci.* **13**, 5849 (2023).
- [28] W.-Q. Sun and D.-M. Yan, Identification of the nonlinear vibration characteristics in hydropower house using transfer entropy, *Nonlinear Dyn.* **75**, 673 (2014).
- [29] Y. Gao, X. Wang, T. Potter, J. Zhang, and Y. Zhang, Single-trial eeg emotion recognition using granger causality/transfer entropy analysis, *J. Neurosci. Methods* **346**, 108904 (2020).
- [30] R. Murcio, R. Morphet, C. Gershenson, and M. Batty, Urban transfer entropy across scales, *PLoS One* **10**, e0133780 (2015).
- [31] S. Ito, Backward transfer entropy: Informational measure for detecting hidden markov models and its interpretations in thermodynamics, gambling and causality, *Sci. Rep.* **6**, 36831 (2016).
- [32] M. Oka and T. Ikegami, Exploring default mode and information flow on the web, *PLoS One* **8**, e60398 (2013).
- [33] S. Ito and T. Sagawa, Information thermodynamics on causal networks, *Phys. Rev. Lett.* **111**, 180603 (2013).
- [34] S. Ito and T. Sagawa, Information flow and entropy production on bayesian networks, arXiv:1506.08519 (2015).
- [35] S. Ito and T. Sagawa, Maxwell's demon in biochemical signal transduction with feedback loop, *Nat. Commun.* **6**, 7498 (2015).
- [36] R. E. Spinney, J. T. Lizier, and M. Prokopenko, Transfer entropy in physical systems and the arrow of time, *Phys. Rev. E* **94**, 022135 (2016).
- [37] P. P. Potts and P. Samuelsson, Detailed fluctuation relation for arbitrary measurement and feedback schemes, *Phys. Rev. Lett.* **121**, 210603 (2018).
- [38] J. M. Horowitz and H. Sandberg, Second-law-like inequalities with information and their interpretations, *New J. Phys.* **16**, 125007 (2014).
- [39] A. Auconi, A. Giansanti, and E. Klipp, Information thermodynamics for time series of signal-response models, *Entropy* **21** (2019).
- [40] J. M. Horowitz, Multipartite information flow for multiple maxwell demons, *J. Stat. Mech.: Theory Exp.* **2015** (3), P03006.
- [41] N. Ruiz-Pino and A. Prados, Entropic balance with feedback control: Information equalities and tight inequalities, *Phys. Rev. Lett.* **136**, 067101 (2026).
- [42] D. Pinna, F. Abreu Araujo, J.-V. Kim, V. Cros, D. Querlioz, P. Bessiere, J. Droulez, and J. Grollier, Skyrmion gas manipulation for probabilistic computing, *Phys. Rev. Appl.* **9**, 064018 (2018).
- [43] J. Zázvorka, F. Jakobs, D. Heinze, N. Keil, S. Kromin, S. Jaiswal, K. Litzius, G. Jakob, P. Virnau, D. Pinna, K. Everschor-Sitte, L. Rózsa, A. Donges, U. Nowak, and M. Kläui, Thermal skyrmion diffusion used in a reshuffler device, *Nat. Nanotechnol.* **14**, 658 (2019).
- [44] R. Ishikawa, M. Goto, H. Nomura, and Y. Suzuki, Implementation of skyrmion cellular automaton using brownian motion and magnetic dipole interaction, *Appl. Phys. Lett.* **119**, 072402 (2021).
- [45] T. Tani, S. Miki, H. Mori, M. Goto, Y. Suzuki, and E. Tamura, Transfer Entropy and Flow of Information in Two-Skyrmion System, *J. Phys. Soc. Jpn.* **95**, 044703 (2026).
- [46] Y. Suzuki, H. Mori, S. Miki, K. Emoto, R. Ishikawa, E. Tamura, H. Nomura, and M. Goto, Information dynamics, natural computing and maxwell's demon in two skyrmions system, arXiv:2506.12881 (2025).
- [47] S. Miki, Y. Jibiki, E. Tamura, M. Goto, M. Oogane, J. Cho, R. Ishikawa, H. Nomura, and Y. Suzuki, Brownian motion of magnetic skyrmions in one-and two-dimensional systems, *J. Phys. Soc. Jpn.* **90**, 083601 (2021).
- [48] L. Zhao, Z. Wang, X. Zhang, X. Liang, J. Xia, K. Wu, H.-A. Zhou, Y. Dong, G. Yu, K. L. Wang, X. Liu, Y. Zhou, and W. Jiang, Topology-dependent brownian gyromotion of a single skyrmion, *Phys. Rev. Lett.* **125**, 027206 (2020).
- [49] Y. Suzuki, S. Miki, Y. Imai, and E. Tamura, Diffusion of a magnetic skyrmion in two-dimensional space, *Phys. Lett. A* **413**, 127603 (2021).
- [50] A. E. Allahverdyan, D. Janzing, and G. Mahler, Thermodynamic efficiency of information and heat flow, *J. Stat. Mech.: Theory Exp.* **2009** (09), P09011.
- [51] J. T. Lizier, M. Prokopenko, and A. Y. Zomaya, Local measures of information storage in complex distributed computation, *Inf. Sci.* **208**, 39 (2012).
- [52] E. Tamura, C. Liu, S. Miki, J. Cho, M. Goto, H. Nomura, R. Nakatani, and Y. Suzuki, Skyrmion confinement and dynamics in tracks patterned with magnetic anisotropy: theory and simulations, arXiv:2005.04860 (2020).
- [53] S. Miki, E. Tamura, H. Nomura, M. Goto, and Y. Suzuki, Size-independent drive of one-dimensional skyrmion motion using exchange energy control, *J. Phys. Soc. Jpn.* **90**, 114703 (2021).
- [54] D. Capic, D. A. Garanin, and E. M. Chudnovsky, Skyrmion-skyrmion interaction in a magnetic film, *J. Phys. Condens. Matter* **32**, 415803 (2020).
- [55] S.-Z. Lin, C. Reichhardt, C. D. Batista, and A. Saxena, Particle model for skyrmions in metallic chiral magnets: Dynamics, pinning, and creep, *Phys. Rev. B* **87**, 214419 (2013).
- [56] U. S. Basak, S. Sattari, M. Hossain, K. Horikawa, and T. Komatsuzaki, Transfer entropy dependent on distance among agents in quantifying leader-follower relationships, *Biophys. physicobiology* **18**, 131 (2021).
- [57] J. Brown, T. Bossomaier, and L. Barnett, Information flow in finite flocks, *Sci. Rep.* **10**, 3837 (2020).
- [58] U. S. Basak, M. E. Islam, and S. Sattari, Inferring interaction domains of collectively moving agents with varying radius of influence, *AIP Adv.* **13**, 035312 (2023).
- [59] K. Hlaváčková-Schindler, M. Paluš, M. Vejmelka, and J. Bhattacharya, Causality detection based on information-theoretic approaches in time series analysis, *Phys. Rep.* **441**, 1 (2007).